Mechanisms of Electrochemical N₂ Splitting by a Molybdenum Pincer Complex

Quinton J. Bruch,[†] Santanu Malakar,[‡] Alan S. Goldman,[‡] Alexander J. M. Miller[†*]

† Department of Chemistry, University of North Carolina at Chapel Hill, Chapel Hill, North Carolina 27599–3290, United States

‡ Department of Chemistry and Chemical Biology, Rutgers, The State University of New Jersey, New Jersey, 08903, United States

ABSTRACT: Molybdenum complexes supported by tridentate pincer ligands are exceptional catalysts for dinitrogen fixation using chemical reductants, but little is known about their prospects for electrochemical reduction of dinitrogen. The viability of electrochemical N₂ binding and splitting by a molybdenum(III) pincer complex, $(^{py}PNP)MoBr_3$ (^{py}PNP = 2,6-bis($^tBu_2PCH_2$)-C_5H_3N)), is established in this work, providing a foundation for a detailed mechanistic study of electrode-driven formation of the nitride complex $(^{py}PNP)Mo(N)Br$. Electrochemical kinetic analysis, optical and vibrational spectroelectrochemical monitoring, and computational studies point to two reaction pathways: in the "reaction layer" pathway, the molybdenum(III) precursor is reduced by $2e^-$ and generates a bimetallic molybdenum(I) $Mo_2(\mu\text{-}N_2)$ species capable of N–N bond scission. In the "bulk solution" pathway the precursor is reduced by $3e^-$ at the electrode surface to generate molybdenum(0) species that undergo chemical redox reactions via comproportionation in the bulk solution away from the electrode surface to generate the same bimetallic molybdenum(I) species capable of N₂ cleavage. The comproportionation reactions reveal the surprising intermediacy of dimolybdenum(0) complex *trans,trans*-$[(^{py}PNP)Mo(N_2)_2]_2(\mu\text{-}N_2)$ in N₂ splitting pathways. The same "over-reduced" molybdenum(0) species was also found to cleave N₂ upon addition of lutidinium, an acid frequently used in catalytic reduction of dinitrogen.

1. INTRODUCTION

The fixation of dinitrogen as ammonia via the Haber-Bosch process (HB) is a critical industrial transformation that underpins the production of synthetic fertilizers. The cost of a process that supports roughly 50% of the global food supply[1,2] is an enormous energy requirement: ca. 2% of annual energy expenditures worldwide. Furthermore, HB relies on H₂ sourced from fossil fuels resulting in ca. 2% of annual CO₂ emissions.[3] This combination of an over-reliance on fossil fuels and massive energy input requirements contextualized against the backdrop of ongoing climate crises has made the pursuit of sustainable industrial NH₃ production a major scientific challenge.

One HB alternative is a fully electrochemical approach that combines N₂ and H⁺ and e^- equivalents derived from water oxidation (**Scheme 1**, top). This approach not only removes the reliance on fossil fuels, but could decentralize NH₃ production and thus avoid requisite CO₂ emissions associated with ammonia distribution.[4,5]

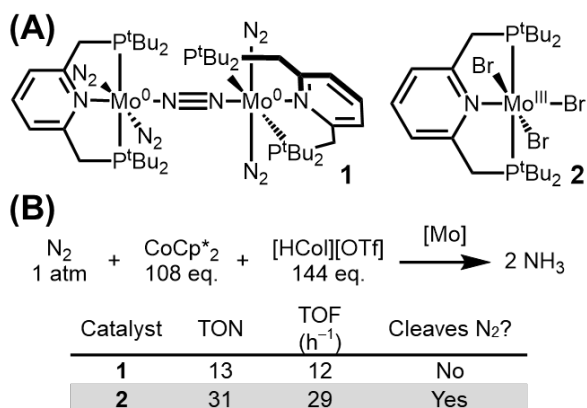**Scheme 1.** Comparison of electrochemical and chemical approaches to dinitrogen fixation.
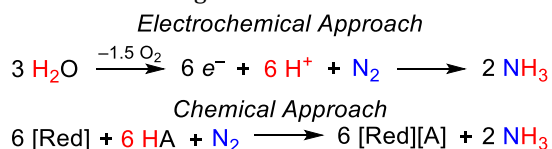
To date, however, the prevailing approach has focused on molecular N₂ fixation catalysts driven by an excess of chemical reductants (**Scheme 1**, bottom). Molybdenum

catalysts have played a particularly prominent role, starting with Schrock's seminal work with trisamido-amine systems[6] and ongoing breakthroughs by Nishibayashi, and others.[7-9] One unifying theme in these molecular catalyst studies is that they all utilize excess chemical reductants under the auspices of later transitioning to electrode-mediated reductions. However, there are very few examples of electrochemical N₂ reduction.[10-15]

The prototypical $(^{py}PNP)Mo$ catalysts (^{py}PNP = 2,6-bis($^tBu_2PCH_2$)-C_5H_3N)) would be an ideal starting point for electrochemical exploration due to their high catalytic activity. The first reported $(^{py}PNP)Mo$ catalyst, the dimolybdenum(0) $[(^{py}PNP)Mo(N_2)_4]_2(\mu\text{-}N_2)$ (**1, Scheme 2A**),[16] has been proposed to undergo distal protonation at one of the terminal N₂ ligands to initiate catalysis via a classical "Chatt cycle" mechanism.[17-20] Catalysts developed later, such as the monometallic molybdenum(III) complex $(^{py}PNP)MoBr_3$ (**2, Scheme 2A**) exhibit higher activity under the same conditions (**Scheme 2B**) and have been proposed to proceed via the N₂ cleavage mechanism in which a *bridging* N₂ ligand splits apart to form the nitride intermediate $(^{py}PNP)Mo(N)Br$.[21,22]

Scheme 2. (A) Examples of active N_2 fixation catalysts supported by the (^{py}PNP) ligand. (B) Comparison of catalyst activity in N_2 fixation under identical conditions. Equivalents of reagents are per Mo center.[21]

(A)

(B)

$$N_2 \quad + \quad CoCp*_2 \quad + \quad [HCol][OTf] \quad \xrightarrow{[Mo]} \quad 2\ NH_3$$
$$1\ atm \qquad 108\ eq. \qquad 144\ eq.$$

Catalyst	TON	TOF (h^{-1})	Cleaves N_2?
1	13	12	No
2	31	29	Yes

The high yields and catalytic activity observed under the N_2 cleavage pathway indicate that **2** would be a prime candidate for investigation of electrochemical reactivity. However, while redox potentials of several (^{py}PNP)Mo species have been reported to date,[20,21] the electrochemical behavior of **2** remains unexplored. It is also unclear whether the chemical reactivity of **2** will readily translate to an electrochemical approach, or if there are unique features of electrochemically driven N_2 activation and splitting for these molybdenum catalysts.

In this study, we demonstrate the viability of electroreductive N_2 splitting by (^{py}PNP)MoBr$_3$ (**2**) and use electroanalytical methods and a suite of spectroelectrochemistry experiments to establish key features of the electrochemical mechanism of N_2 activation and splitting into nitride complexes. Herein we identify two pathways which rely on monometallic-bimetallic equilibria to gate reactivity at the electrode surface and minimize the necessary applied potentials. We also establish the essential role of *chemical redox reactions* far from the electrode surface, which activate the *electrochemically produced* "over-reduced" Mo^0 complex **1** towards N_2 splitting. Given that complex **1** was previously thought to follow an independent path of N_2 reduction that does not rely on N_2 cleavage, its observation during electrochemical N_2 splitting helps identify a potentially broader role of Mo^0 complexes as electron reservoirs in both chemical and electrochemical N_2 reduction to NH_3.

2. RESULTS AND DISCUSSION

2.1 Electrochemical reactivity of (^{py}PNP)MoBr$_3$ under Ar and N_2.

Initial cyclic voltammograms (CVs) of (^{py}PNP)MoBr$_3$ (**2**) were recorded under Ar and N_2, revealing a clear impact of the atmosphere on the electrochemical behavior (**Figure 1A-1B**). Therefore, the behavior of **2** was studied in more detail under both Ar and N_2 to elucidate when and how chemical reactions with N_2 occur upon reduction. In this section we discuss the behavior of the first reduction feature, see SI Section VIII for investigation of additional reduction events.

CVs of **2** under Ar at scan rates (v) below 10 V/s present a completely irreversible reduction around –1.81 V (all potentials are reported versus Fc$^{+/0}$ unless otherwise stated) that shifts anodically at slower scan rates (**Figure 1A**). The CVs also contain an irreversible oxidation (ca. –1.27 V) that is only present in the return sweep that shifts cathodically at slower scan rates. At $v \geq 20$ V/s, the reduction feature becomes partially reversible ($E_{1/2} \approx -1.85$ V, **Figure S38**), with peak-to-peak separations consistent with a 1e$^-$ process (ΔE_p(Mo) = 299 mV, ΔE_p(FeCp*$_2$) = 261 mV).

The observed electrochemical behavior is indicative of an EC process (electrochemical step followed by chemical step) wherein 1e$^-$ reduction of **2** under Ar yields [(^{py}PNP)MoBr$_3$]$^-$ (**2$^-$**, **Figure 1D**). Subsequent loss of Br$^-$ from **2$^-$** would yield (^{py}PNP)MoBr$_2$ (**3**). Dissociation of Br$^-$ was explored electrochemically by recording CVs of **2** with varying concentrations of added Br$^-$ (**Figure 1C**). At 25 mV/s, the oxidation feature at ca. –1.27 V disappears as the concentration of Br$^-$ increases. At the same time, the reduction becomes seemingly reversible, confirming the chemical step to be bromide-coupled (C$_{Br}$). Using the $E_{1/2}$ and the scan rate-dependent shift in E_{pc}, the forward rate constant (k_f) of C$_{Br}$ was estimated to be 400 s^{-1} ± 100 s^{-1} (**Figure S39**).[23,24] The observed electrochemical behavior could also be appropriately simulated after inclusion of a reversible THF binding step to generate (^{py}PNP)MoBr$_2$(THF) (**3-THF**) with an overall experimentally estimated free energy of bromide-THF exchange as –2 kcal/mol (see SI Section VIII). Computations further support the C$_{Br}$ step, as DFT predicts Br$^-$ loss to be exergonic (computed $\Delta G_{Br,diss}°$ = –2 kcal/mol, see SI Section XII). The iodide analogue of **3**, (^{py}PNP)MoI$_2$, was also recently synthesized by reducing (^{py}PNP)MoI$_3$ with CoCp*$_2$ (Cp* = pentamethylcyclopentadienyl) under Ar.[25]

Moving to an N_2 atmosphere has a marked impact on the electrochemical response. Under N_2, the first reduction feature of **2** was found to be partially reversible at fast scan rates ($E_{1/2} \approx -1.86$ V). At moderate scan rates ($5 \leq v \leq 10$ V/s), EC behavior was observed with an experimentally determined k_f of 370 s^{-1} ± 100 s^{-1} (see SI Section VIII). The estimated $E_{1/2}$ at fast scan rates and the rate constant are within error of the values determined under Ar ($E_{1/2} \approx -1.85$ V, k_f = 400 s^{-1} ± 100 s^{-1}), suggesting that C$_{Br}$ is the first chemical step under N_2. As the scan rate was further slowed ($v \leq 1000$ mV/s), E_{pc} shifted anodically and $i_{pc}/\sqrt{v}$ increased (**Figure 1B**) suggesting additional reactivity with N_2 was taking place. Based on the proposed structure of **3**, initial N_2 binding to yield (^{py}PNP)MoBr$_2$(N_2) (**3-N_2**, **Figure 1D**) is reasonable, with N_2 binding computed to be slightly endergonic (6 or 7 kcal/mol to form the *cis* or *trans* isomer, respectively). The observed increase in $i_{pc}/\sqrt{v}$ indicates that more than 1e$^-$ during the first reduction feature under N_2, likely due to additional reductions of **3-N_2** once it forms at
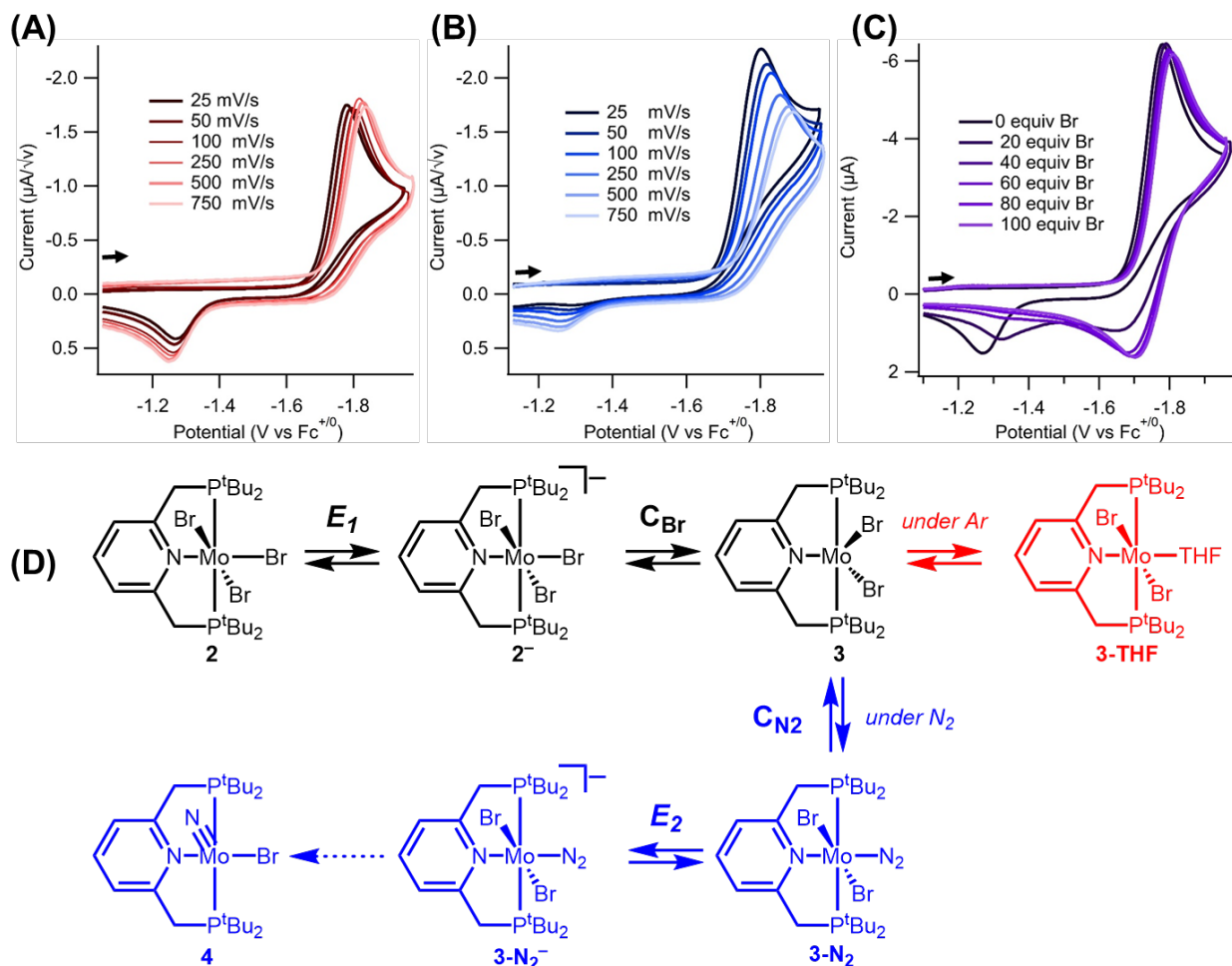
Figure 1. CVs of 1 mM (pyPNP)MoBr$_3$ (**2**) in 0.2 M [nBu$_4$N][PF$_6$] in THF (A) under Ar sweeping cathodically at varying scan rates, (B) under N$_2$ sweeping cathodically at varying scan rates, and (C) under Ar sweeping cathodically at 25 mV/s with varying [Br$^-$]. (D) Proposed mechanisms upon reduction of **2** under Ar (top, red) and under N$_2$ (bottom, blue). $E_2 > E_1$.

the electrode surface via "potential inversion" ($E_2 > E_1$). This behavior can be attributed to the π-acidic nature of the N$_2$ ligand causing dramatic anodic shifts in reduction potentials of M(N$_2$) species relative to M.[12,15,26-32]

The voltammetric studies together provide clear evidence for an initial sequence of electroreduction-induced bromide dissociation and N$_2$ association, followed by additional electron transfer steps.

2.2   Electrochemical N$_2$ Splitting. To establish the products of the electroreduction under N$_2$, controlled potential electrolysis (CPE) was carried out on a 4 mM solution of **2** in THF under N$_2$ near the first reduction peak potential (E_{appl} = −1.89 V vs Fc$^{+/0}$). Over the course of the electrolysis, two 'zones' of current response were observed and corresponded to color changes from orange to blue to green as the charge equivalent of 2 e^- per Mo center was passed (**Figure 2B**). Analysis of the resulting catholyte revealed the desired molybdenum nitride product (pyPNP)Mo(N)Br (**4**) was formed in 41% ± 1% yield according to ^{1}H NMR spectroscopy (**Figure 2A**). In addition to **4**, the over-reduced Mo^0 species [(pyPNP)Mo(N$_2$)$_4$]$_2$(μ-N$_2$) (**1**) could also be detected in trace quantities (< 2%). The

nitride product must be formed by an N$_2$ splitting reaction, given that no proton source was added to the electrochemical cell. There are no reported examples of electroreductive N$_2$ splitting at Mo; but electro-oxidative N$_2$ splitting by *trans*-(depe)$_2$Mo(N$_2$)$_2$ was recently reported.[14]

Having demonstrated that electrochemical N$_2$ splitting was feasible, N$_2$ splitting with chemical reductants was targeted next. CoCp*$_2$ was selected due to the similarity between its reduction potential ($E_{1/2}$ = −1.85 V in THF, **Table S1**) and E_{appl}. Addition of 3.3 equiv of reductant to **2** in THF-d_8 results in the formation of an intensely blue solution and a yellow-brown insoluble [CoCp*$_2$][Br]. After 16 h, the solution remained an intensely blue color and the molybdenum nitride species **4** was detected in 20% yield by ^{1}H NMR spectroscopy. The bimetallic Mo^0 **1** was not detected, but free pyPNP ligand was found (6% yield) as well as trace unidentified diamagnetic species (14%).
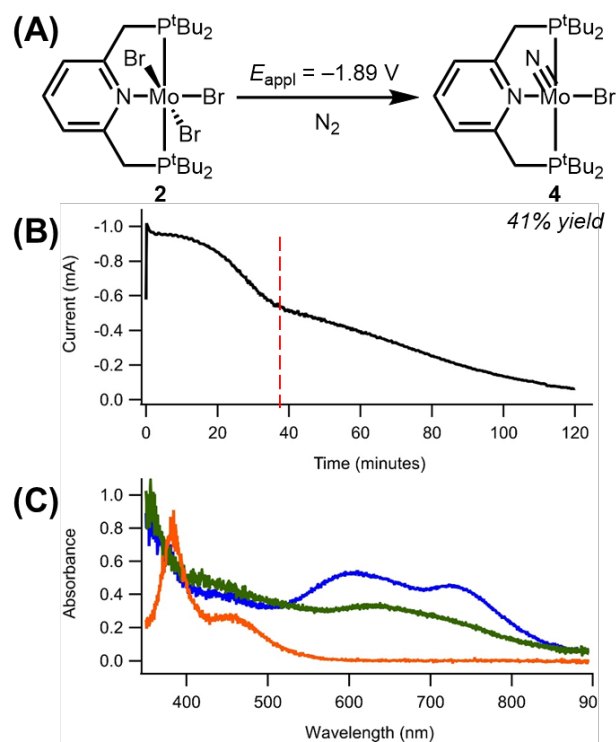
Figure 2. (A) Electrochemical N_2 splitting upon reduction of $(^{py}PNP)MoBr_3$ (**2**) to yield $(^{py}PNP)Mo(N)Br$ (**4**). (B) CPE trace during the reduction of **2** (4 mM) in THF (0.2 M $[^nBu_4][PF_6]$) under an N_2 atmosphere. Red dashed line marks the start of the color change from blue to green. (C) UV-Vis spectra of the bulk solution during the CPE reduction of **2** at 0 min (orange), 45 min (blue), and 120 min (green).

Excitingly, the yield of the desired Mo(N) was higher during electrochemical reductions. Additionally, the appearance of two "zones" during the CPE and two distinct color changes hints at the formation of detectable intermediates. To search for and characterize these intermediates, CPE of **2** was carried out under the same conditions used above but with aliquots taken from the bulk solution for IR and UV-Vis spectroscopic measurements every 5-10 minutes.

During the first "zone", the solution turns from orange to blue and UV-Vis analysis revealed the formation of new absorbances (λ_{max} = 600 and 729 nm) over the first 45 min of electrolysis (**Figure 2C**, blue). During this time, charge correlating to 1.3 e^- per Mo was passed, suggesting the blue-colored intermediate is a one-electron reduction product. Continued monitoring (45 to 120 minutes) revealed the intermediate to be transient, as yet another species with a broad shoulder centered at 633 nm was detected as the solution turned from dark blue to dark green as an additional ca. 0.7 e^- (2.0 e^- equiv total) were passed (**Figure 2C**, green). Throughout the course of the experiment, no terminal N_2 stretches were detected by IR spectroscopy.

2.3   Synthesis and Electrochemical Reactivity of an Isolable Mo^{II} Intermediate. To further investigate the initial intermediate formed, one-electron reduction of **2** was explored using chemical reductants. Addition of 1 equiv of

CoCp*$_2$ to **2** at –30 °C in THF resulted in rapid formation of a dark red solution that slowly turned dark blue over the course of 30 min at –30 °C (**Scheme 3**). Analysis of the isolated solid via UV-Vis revealed nearly identical absorbance features (λ_{max} = 606 and 730 nm) to those detected during electrochemical reduction (**Figure 2C, blue**).

Scheme 3. Synthesis of *trans,trans*-$[(^{py}PNP)MoBr_2]_2(\mu\text{-}N_2)$ (**5^{t,t}**).
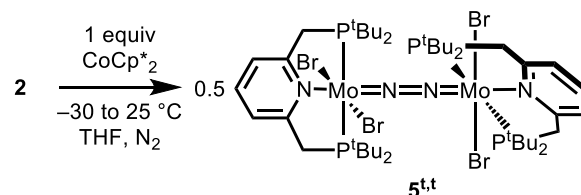
NMR spectroscopy in THF-d_8 revealed the species to be paramagnetic and no $(^{py}PNP)Mo(N)Br$ was detected. Evans Method measurements yielded a solution magnetic moment, μ_{eff}, of 5.4, which is similar to the expected spin only value of a quintet state ($\mu_{s.o.}$ = 4.9). Saturated THF solutions of the blue solid revealed no terminal ν_{NN} stretches by IR spectroscopy while resonance Raman (rR) spectra contained features at 1595 and 1751 cm^{-1}. The feature at 1751 cm^{-1} was assigned to a bridging N_2 ligand while the stretch at 1595 cm^{-1} was assigned to the (^{py}PNP) ligand (*vide infra*).[33,34] Single crystals grown via vapor diffusion of pentane into a saturated toluene solution at 25 °C allowed for unambiguous assignment as the N_2-bridged bimetallic Mo^{II} species, *trans,trans*-$[(^{py}PNP)Mo(Br)_2]_2(\mu\text{-}N_2)$ (**5^{t,t}, Figure 3**). The solid state structure of **5^{t,t}** is similar to the tetrachloride analogue,[35] and contains a modestly activated N_2 ligand (N–N bond distance of 1.160(3) Å versus 1.110 Å in free N_2[36]) which aligns with the measured ν_{NN} stretching frequency.[36]
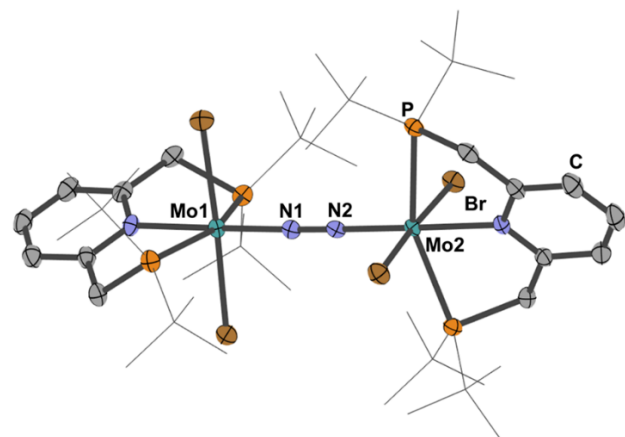

Figure 3. Structural representation of *trans,trans*-$[(^{py}PNP)MoBr_2]_2(\mu\text{-}N_2)$ (**5^{t,t}**) from singe crystal X-ray diffraction with ellipsoids set at 50% occupancy. For clarity, hydrogen atoms were omitted and ^tBu substituents are wire-framed for improved visibility. Select bond distances (Å): Mo1–N1: 1.926(2); N1–N2: 1.160(3); Mo2–N2:

1.926(3). Select angle (°): Mo1-N1-N2: 178.7(2), Mo2-N2-N1: (175.9(2). See SI Section XIII for more details.

Although dimolybdenum(II) complex $5^{t,t}$ contains the desired end-on bridging N_2 binding mode needed for N_2 splitting, $5^{t,t}$ is stable both in the solid and solution state for weeks at a time. The N_2-bridged complex $5^{t,t}$ is therefore not kinetically competent for N_2 splitting on the ca. 2 h timescale of the CPE experiments.

Having ruled out direct N_2 splitting from $5^{t,t}$ itself, we hypothesized that further reduction would be needed to furnish the nitride product. The electrochemical behavior of the proposed intermediate was therefore explored next. Starting with CVs of $5^{t,t}$ under an N_2 atmosphere, sweeping reductively revealed a minor feature at ca. –1.84 V that passed significantly less current than the major reduction feature around –2.16 V (**Figure 4A**). The minor feature at –1.84 V is similar to where the reduction of **2** occurs; however, trace **2** could be ruled out as an impurity based on comparisons of CVs of **2** and $5^{t,t}$ under Ar where it is clear that the return oxidation feature at ca. –1.27 V is absent (**Figure S54**). Scan rate dependency studies of $5^{t,t}$ under N_2 and Ar revealed the major reduction feature at ca. –2.16 V to be an EC process under Ar and an $EC_{N_2}E$ process under N_2 (**Figure 4A**, see SI section IX for more details). These studies also revealed that the prewave feature at ca. –1.84 V shifted anodically while $i_{pc}/\sqrt{v}$ increased at slower scan rates, hallmark signs of a CE process. Based on the structure of $5^{t,t}$, we attribute the chemical step to a dissociation of the bimetallic $5^{t,t}$ coupled with binding of N_2 to yield the monometallic species $3\text{-}N_2$. This monometallic-bimetallic equilibrium shown in **Figure 4B** was computationally explored, and found to be only modestly endergonic at room temperature ($\Delta G_{5t,tdiss}° = 5$ kcal/mol, see SI Section XII).

(A)

(B)
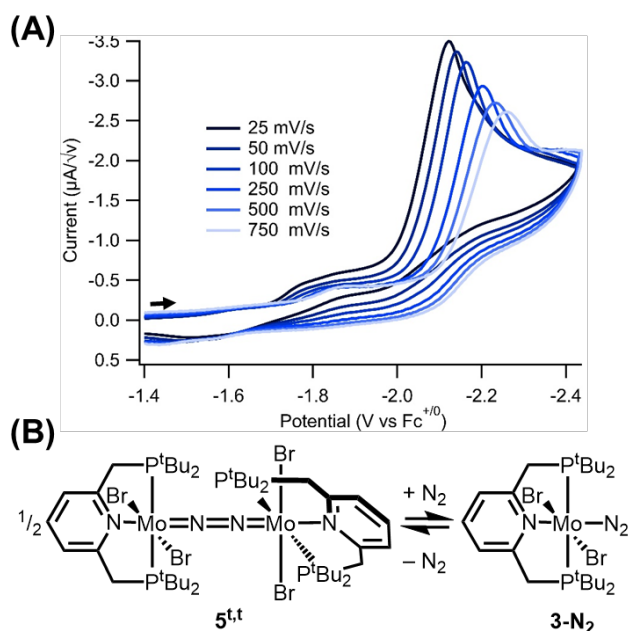
Figure 4. (A) CVs of of 1 mM *trans,trans*-[(^{py}PNP)MoBr$_2$]$_2$(μ-N_2) ($5^{t,t}$) under N_2 sweeping cathodically at varying scan rates. (B) Proposed monometallic-bimetallic equilibrium as the chemical step in the CE prewave process.

Considering the CVs in **Figure 4** in the context of CPE-driven N_2 splitting, we found that the potential applied during CPE (–1.89 V) aligns with the *prewave* CE feature of $5^{t,t}$ (–1.84 V), rather than the main reduction of $5^{t,t}$ (–2.16 V). Therefore, CPE of **2** was carried out at an applied potential of –2.11 V under N_2, a potential where intermediate $5^{t,t}$ would be reduced rapidly (**Table 1**). Surprisingly, the yield of the Mo(N) product **4** *decreased* from 41% to 17% and several unidentified diamagnetic Mo products were observed (**Figure S26**).

To further probe the potential dependence of N_2 splitting, CPE of 2 mM solutions of $5^{t,t}$ ([Mo]$_{total}$ = 4 mM) to generate **4** was carried out under N_2 at the E_{pc} of both the prewave CE feature and the main reduction feature (**Table 1**). Notably, yields of **4** were lower from the reduction of the apparent intermediate $5^{t,t}$ than from the direct reduction of **2** and, once again, at milder potentials, the yield of **4** was substantially higher (22% versus 3%, at -1.89 V and -2.11 V respectively, **Table 1**). Finally, because $5^{t,t}$ contains a pre-coordinated N_2 ligand, CPE under Ar could also yield the Mo(N) product **4**. Remarkably, the electrochemical yields of **4** upon electrolysis of $5^{t,t}$ under Ar were markedly higher than under N_2 (41% vs. 22% at –1.89 V, 43% v 3% at –2.11 V).

Table 1. Electrochemical reduction of (^{py}PNP)Mo(N)Br (**4**) under varying conditions.

(^{py}PNP)Mo precursor	Atm	E_{appl}	% Yield of (^{py}PNP)Mo(N)Br[a]
2	N_2	–1.89 V	41% ± 1%
2	N_2	–2.11 V	17%
2	Ar	–1.89 V	0%
$5^{t,t}$	N_2	–1.89 V	22%
$5^{t,t}$	N_2	–2.11 V	3%
$5^{t,t}$	Ar	–1.89 V	42%
$5^{t,t}$	Ar	–2.11 V	43%

[a]Yields of **4** were calculated using the concentration of **4** determined by ^1H NMR spectroscopy and the total concentration of Mo starting material used (i.e. [Mo]$_{total}$ = [**2**] = 2 × [$5^{t,t}$]).

The yields of **4** reported in **Table 1** clearly demonstrate a strong dependence on all three parameters: (^{py}PNP)Mo precursor, atmosphere, and applied potential. Under Ar, N_2 cleavage is only observed when it is pre-incorporated in $5^{t,t}$. Intriguingly, the yields of **4** from $5^{,t,t}$ under Ar are not impact by applied potential *and* they are substantially higher than under N_2. This suggests that the ability for reduced Mo species to interact with additional N_2 molecules may be detrimental to the desired N_2 cleavage reaction.

2.4 Spectroelectrochemical Identification of Low Valent Mo⁰ Intermediates. To directly probe the Mo species formed at the surface of the electrode, spectroelectrochemistry (SEC) studies were carried out on 4 mM solutions of **2** in 0.2 M [^{n}Bu$_4$][PF$_6$] solutions in THF under an N$_2$ atmosphere. A thin-layer transmission cell with a Au mini-grid working electrode was used for both IR and rR spectroeletrochemistry,[37] and a short pathlength cuvette fitted with a honeycomb Au working electrode was used for UV-Vis spectroelectrochemistry. In all cases (IR, rR, UV-Vis) a progressively more negative potential was applied, stepping –0.1 V every 120 seconds.

Monitoring the products formed at the surface of the electrode by IR spectroscopy revealed the formation of a dominant feature at 1944 cm^{-1} as well as a shoulder at 1963 cm^{-1} and a minor stretch at 2043 cm^{-1} (**Figure 5A**). While this clearly indicates the formation of terminal Mo(N$_2$) species, the generation of known intermediates such as **5^{t,t}** featuring symmetric bridging N$_2$ ligands would not be detected, as they are IR silent. Therefore, the rR spectrum was also monitored over the same potential range. Using a Raman Microscope equipped with a 633 nm laser, electrolysis of **2** resulted in the initial formation of stretches at 1595, 1684, and 1751 cm^{-1} (**Figure 5A**). The features at 1595 and 1751 cm^{-1} clearly align with the Mo^{II} species **5^{t,t}**,

while the feature at 1680 cm^{-1} is likely an isomer of **5^{t,t}**, as the shift to more activated N$_2$ stretches has been previously observed in Re$_2$(μ-N$_2$) complexes and is computational predicted upon isomerization of *trans,trans* M$_2$(μ-N$_2$) species.[38,39] Additionally, monitoring the chemical reduction of **2** with 1 equiv of CoCp*$_2$ via rR revealed a minor feature at ca. 1680 cm^{-1} that decayed alongside concomitant growth of the feature at 1751 cm^{-1} that corresponds to **5^{t,t}** (**Figure S9**). Ultimately, these bimetallic Mo^{II} species proved to be transient, as at more negative potentials features at 1583, 1894, and 2020 cm^{-1} dominated the rR spectrum (**Figure 5A**). Repeating these experiments under an Ar atmosphere led to no IR features from 2200 to 1800 cm^{-1} and only a rR stretch at 1574 cm^{-1} which was attributed to the ^{py}PNP ligand (**Figure S72**).[33,34] While starting solutions of **2** do not show rR stretches in this region, we attribute this to the inability of **2** to efficiently absorb 633 nm light (vide infra).

UV-Vis SEC carried out under identical conditions resulted in increased absorbance between 400 and 900 nm that coalesced into a single broad feature at 684 nm (**Figure 5A**). It is important to note that the UV-vis spectra acquired using the honeycomb electrode, which provides insight into the species in the vicinity of the surface of the electrode, are distinct from the spectra of aliquots taken during a standard
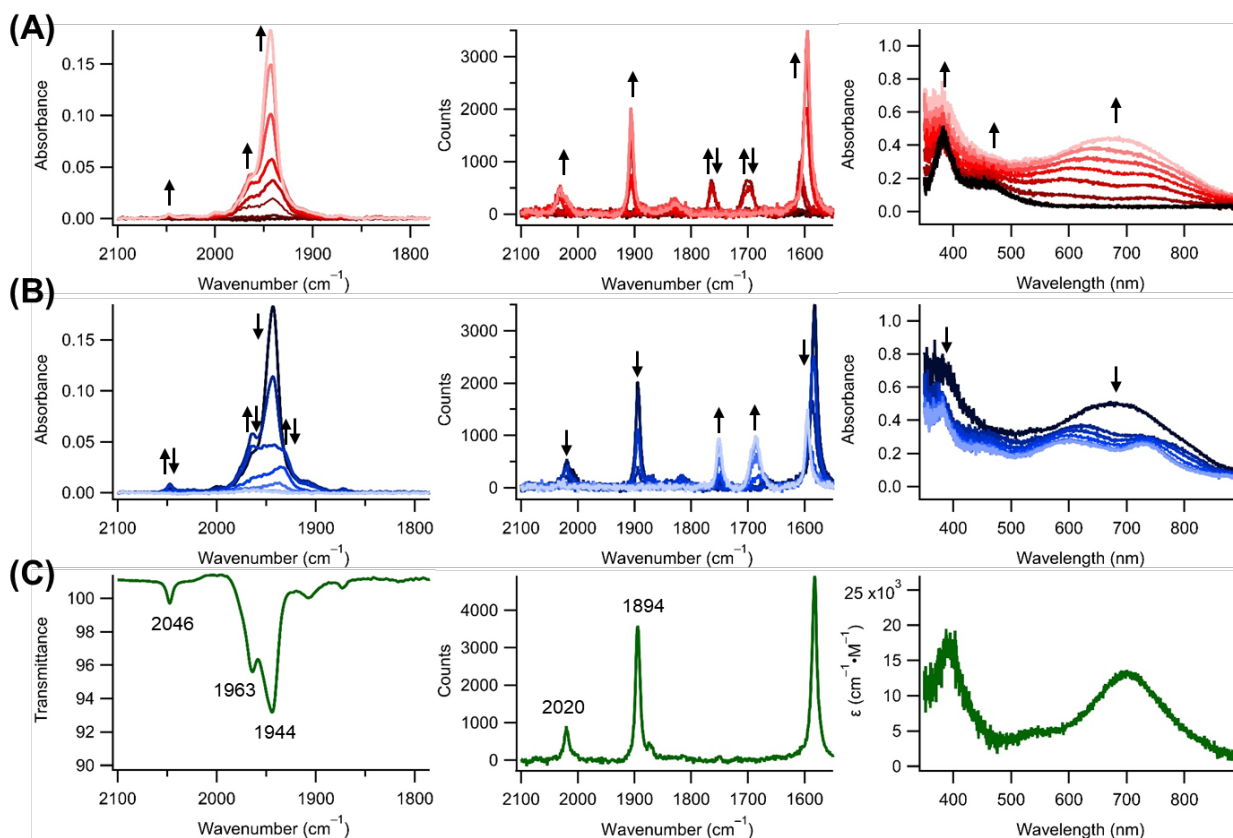
Figure 5. (A) Stepped potential spectroelectrochemical experiments from –0.5 to –1.5 V (vs Ag$^{+/0}$) of 4 mM (^{py}PNP)MoBr$_3$ (**2**) in 0.2 M [^{n}Bu$_4$][PF$_6$] in THF under N$_2$ monitoring by IR (left) rR (middle) and UV-Vis (right). (B) Monitoring the consumption of electrode-generated [(^{py}PNP)Mo(N$_2$)$_2$]$_2$(μ-N$_2$) (**1**) over time, recording spectra every 5 minutes by IR (left, 30 min), rR (middle, 40 min), and UV-Vis (right, 30 min). (C) Authentic IR, rR, and UV-Vis of freshly prepared *trans,trans*-[(^{py}PNP)Mo(N$_2$)$_2$]$_2$(μ-N$_2$) (**1**). Peaks marked with arrows pointing in both directions are transient.

bulk electrolysis experiment (see above). The major species with λ_{max} = 684 nm was confirmed to be a Mo(N$_2$) complex, as UV-Vis SEC under Ar revealed new λ_{max} features at 354 nm and a broad shoulder centered at 500 nm that slowly decays into the red (**Figure S64**).

Over the course of the spectroelectrochemical measurements, all three spectroscopic probes are consistent with formation of the dimolybdenum(0) complex **1** at the electrode surface: [(^{py}PNP)Mo(N$_2$)$_2$]$_2$(μ-N$_2$) has a reported IR stretch at 1944 cm^{-1} (dominant IR SEC feature) and a rR stretch at 1894 cm^{-1} (dominant rR SEC feature).[16] Furthermore, **1** was prepared by reducing **2** with 3 equiv of KC$_8$ and authentic spectra closely matched all SEC data (**Figure 5C**). Unexpectedly, the authentic spectra of **1** also contained features at 1963 and 2046 cm^{-1}, aligning with minor features observed during IR SEC experiments. We assign these features to a monometallic species, (^{py}PNP)Mo(N$_2$)$_3$ (**6**) because IR spectra of recrystallized **1** under N$_2$ showed equilibration between features at 2047, 1963, and 1942 cm^{-1} while under Ar no change was observed (**Figure S8**). Similar monometallic-bimetallic equilibria have been previously reported in a number of d^6 (pincer)Mo(N$_2$) systems,[20,40,41] and the **1/6** equilibria was calculated to be fairly accessible at room temperature ($\Delta G_{1,\text{diss}}^{\circ}$ = 0.2 kcal/mol, see SI Section XII).

The formation of **1** was found to be independent of applied potential, as even at mild potentials corresponding to the foot of the wave of the reduction of **2**, SEC experiments still showed transient formation of **5^{t,t}** followed by the appearance of **1** (see SI Section XI). Accordingly, SEC experiments using **5^{t,t}** in place of **2** also generate **1** at the surface of the electrode, which aligns with reduction of **2** and **5^{t,t}** passing through the common intermediate, **3-N$_2$** (vide supra).

2.5 Role of Chemical Redox Reactions in N$_2$ Cleavage. *2.5.1 Detection of comproportionation reactions with electrode-generated Mo^0 species.* The observation that the dominant electrode-generated species are Mo^0 is highly surprising, as **1** is stable with respect to N$_2$ cleavage. Additionally, the detected yields of **1** after CPE are quite low (<2%), suggesting that it also serves as an intermediate in the N$_2$ cleavage reaction. This is supported by past reports of electrochemical N$_2$ cleavage at rhenium, wherein comproportionation between starting material and over-reduced Re species was critical.[12,15] To determine whether similarly analogous transformations between **2** and Mo^0 species were feasible, IR, rR, and UV-Vis spectra were recorded in the absence of an applied potential immediately concluding stepped potential SEC experiments.

Monitoring the diffusion-limited reaction between surface-generated Mo^0 and bulk **2** in the starting material by IR spectroscopy revealed the rapid consumption of **1** followed by the slower consumption of **6** as a new transient feature appeared at 1932 cm^{-1} (**Figure 5B**). Similarly, rR monitoring revealed the consumption of **1** while features at

1595, 1680, and 1751 cm^{-1} returned, indicative of the formation of **5^{t,t}** (1595 and 1751 cm^{-1}) upon mixing of Mo^0 species and **2** (**Figure 5B**). The post-CPE UV-Vis also clearly revealed the formation of Mo^{II} species, as the bimodal λ_{max} features of **5^{t,t}** at 595 and 730 nm appeared overtime. The observation of **5^{t,t}** also aligns with the detection of **5^{t,t}** in the bulk solution during CPE, as the stirring of the solution serves to increase the rate at which **1** generated at the electrode surface can reaction with unreduced **2**.

The reappearance of **5^{t,t}** after removal of an applied potential bias clearly demonstrates that comproportionation reactions are occurring in which **2** acts as a net Br$^{\bullet}$ donor to **1**, thus generating Mo^I species that are critical for N$_2$ cleavage. In fact, the formation of *cis,cis*-[(^{py}PNP)MoBr]$_2$(μ-N$_2$) (**7^{c,c}**, **Scheme 4** top, here *cis* refers to the relationship between the bridging N$_2$ ligand and the pyridyl central donor) via comproportionation was computed to be endergonic ($\Delta G_{2,\text{comp}}$ = 17 kcal/mol, for $^3/_2$ equivalents of **7^{c,c}**) with subsequent N$_2$ cleavage being strongly exergonic (per Mo(N) formed, $\Delta G_{\text{cleave}}^{\circ}$ = –24 kcal/mol, $\Delta G_{\text{cleave}}^{\ddagger}$ = 19 kcal/mol). Therefore, the chemical redox reaction between **1** and **2** was carried out in 0.2 M [^{n}Bu$_4$N][PF$_6$] in THF-d_8 in the complete absence of an applied potential to allow for detection of **4** by NMR spectroscopy (**Scheme 4**, top). Upon addition of **2** to a green solution of **1**, a dark blue solution forms as **1** is completely consumed based on ^{1}H and ^{31}P{^{1}H} NMR spectroscopy and the N$_2$ cleavage product **4** was detected in 11% spectroscopic yield at 7h (13% at 40 h). UV-Vis of the resultant solution revealed the dark blue color to be due to the formation of **5^{t,t}**, aligning with the SEC data and neither free ligand nor unidentifiable diamagnetic products were detected by ^{31}P{^{1}H} NMR spectroscopy.

The detection of **4** upon reaction of **1** and **2** indicate that this is a viable pathway to cleave N$_2$ during CPE. We also hypothesized another pathway for the formation of **4** via a chemical redox reaction between **5^{t,t}** and **1** (**Scheme 4** bottom), based on SEC data indicating that reduction of **5^{t,t}** generates **1** at the electrode surface. Once again, computations suggest that formation of **7^{c,c}** is slightly uphill ($\Delta G_{5t,t,\text{comp}}$ = 26 kcal/mol, for 2 equivalents of **7^{c,c}**), followed by highly exergonic N$_2$ splitting. Gratifyingly, monitoring the comproportionation between **5^{t,t}** and **1** via NMR spectroscopy under identical conditions to those employed above also resulted in complete consumption of **1** and formation of **4** (27% spectroscopic yield at 7h, increases to 45% at 40 h).

Scheme 4. Comproportionation reactions between $[(^{py}PNP)Mo(N_2)_2]_2(\mu\text{-}N_2)$ (**1**) and either $(^{py}PNP)MoBr_3$ (**2**) or *trans,trans*-$[(^{py}PNP)Mo(N_2)Br_2]_2(\mu\text{-}N_2)$ (**5^{t,t}**) in 0.2 M $[^nBu_4][PF_6]$ under N_2. Note that bimetallic species **1** and **5^{t,t}** are in equilibrium with monometallic **6** and **3**. Complex **7^{c,c}** is proposed to precede N_2 cleavage, but was not detected experimentally. [a]Percent yield was calculated using the quantified concentration of **4** and the total concentration of all Mo, $[\mathbf{4}]/[Mo]_{total}$ (i.e. $[Mo]_{total} = [\mathbf{2}] + 2 \times [\mathbf{1}]$ or $2 \times ([\mathbf{5}^{t,t}] + [\mathbf{1}])$).
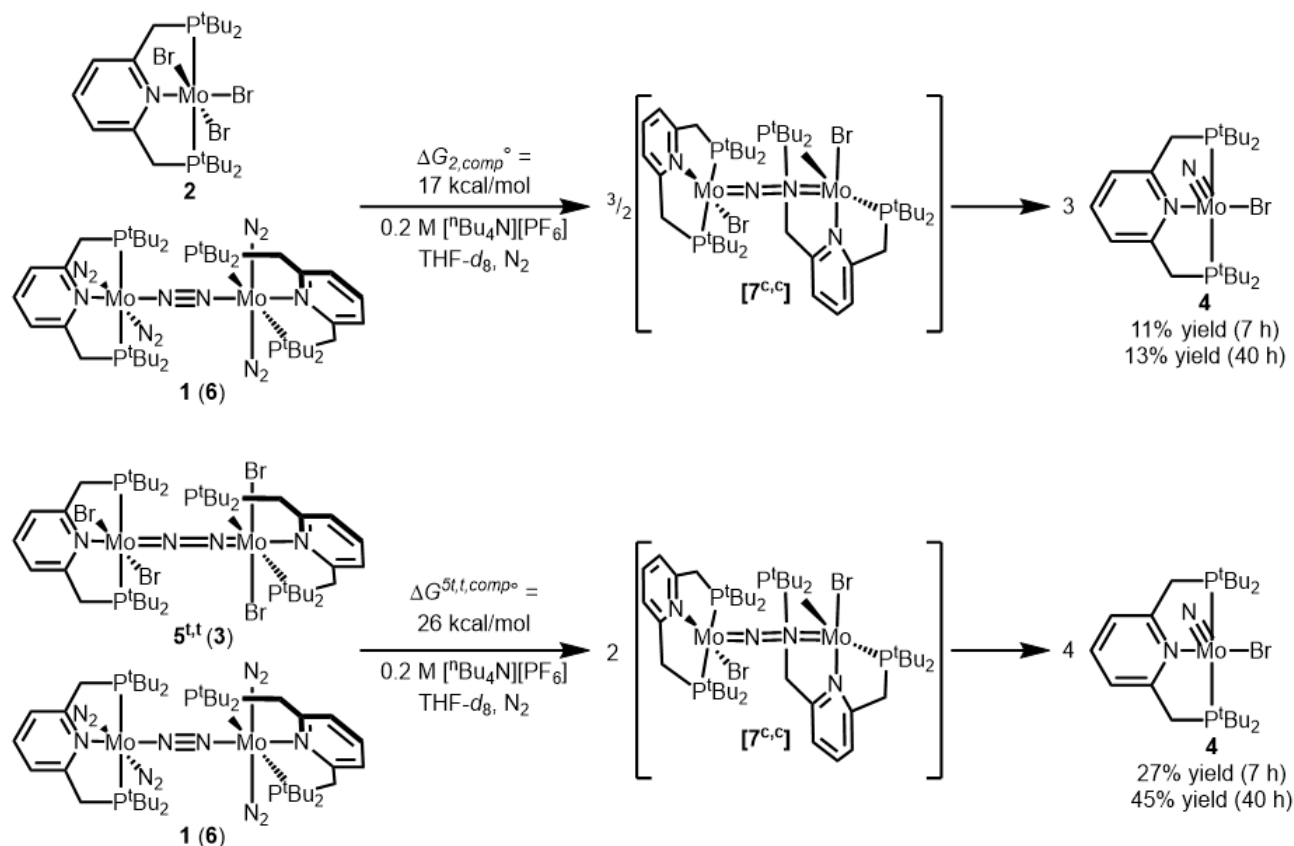
These results unequivocally show that comproportionation reactions between low-valent Mo^0 species and both Mo^{II} and Mo^{III} species are capable of driving N_2 cleavage reactions. The observation of this chemically-driven oxidation of **1** resulting in N_2 splitting is reminiscent of the recently reported (electro)oxidation-induced N_2 cleavage by *trans*-(depe)$_2$Mo(N$_2$)$_2$.[14] Further contextualized with previous studies of (PNP)Re electroreductive N_2 cleavage,[12,15] these results suggest that over-reduction and subsequent comproportionation may be quite common in N_2 splitting mechanisms. Additionally, it is important to note that these chemical redox reactions are sufficiently slow so that they are only observed *away* from the electrode surface;[42] suggesting that the spatial separation afforded by an electrochemical approach (i.e. electrode equivalents only available at the electrode surface) is playing a critical role in the overall mechanism.
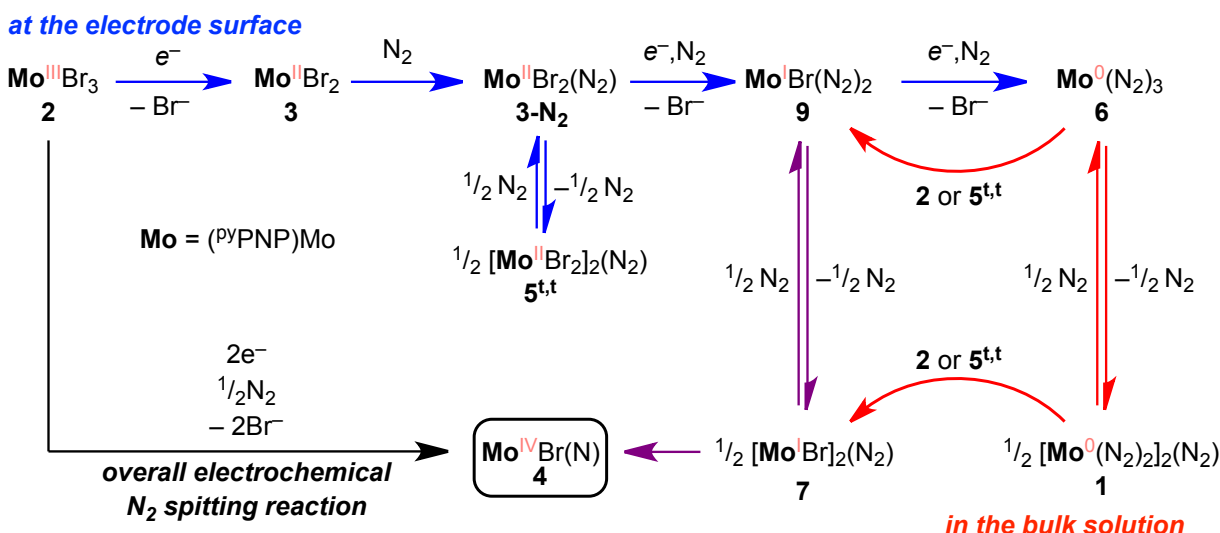
2.5.2 Implications for N_2 fixation catalysis. The ability of **2** and **5^{t,t}** to act as chemical oxidants capable of drawing Mo^0 species onto the N_2 splitting pathway led us to consider other oxidation reactions. One particularly relevant transformation would be the oxidative protonation of Mo^0 species, as molecular acids are already used during N_2 fixation catalysis. Previously, protonation of **1** with HBF$_4$·Et$_2$O in the presence of pyridine resulted in isolation

of a hydrazido complex supported by an additional pyridine ligand.[16] The formation of a Mo(N) product was not reported. Herein, we targeted similar reactivity but used [HLut][Br], as lutidine is less coordinating than pyridine and the use of a bromide counteranion would generate the nitrido bromide complex **4**.

Upon addition of one equivalent of [HLut][Br] to a THF-d_8 solution of **1**, complex **1** was completely consumed and **4** could be detected in 40% yield by ^{1}H NMR spectroscopy. No NH_4^+ was detected, suggesting that the nitride did not originate from NH_3 release upon protonation of a distal nitrogen atom. This demonstrates that protonation is a viable pathway to convert low-valent Mo^0 species to more reactive Mo(N) intermediates via N_2 splitting. The site of protonation of a low-valent N_2 complex can be thought of as setting the N_2 fixation pathway: protonation at the distal nitrogen of a terminal N_2 ligand would lead to a distal (or alternating) mechanism, while protonation at the metal center can increase the formal oxidation state and lead to N_2 cleavage pathways for N_2 fixation.

2.6 Constructing Pathways of Electrochemical N_2 Cleavage. The combined electrochemical and spectroscopic data are consistent with *two interconnected pathways* for electrochemical N_2 cleavage by (PNP)MoBr$_3$ (**2**). As shown

Scheme 5. Proposed mechanisms for electroreductive N_2 cleavage by $(^{py}PNP)MoBr_3$ (**2**), with reactions that occur at the electrode surface (blue), reactions that occur in bulk solution (red), and reactions that occur in both locations (purple).

at the electrode surface

$$Mo^{III}Br_3 \xrightarrow[-Br^-]{e^-} Mo^{II}Br_2 \xrightarrow{N_2} Mo^{II}Br_2(N_2) \xrightarrow[-Br^-]{e^-,N_2} Mo^IBr(N_2)_2 \xrightarrow[-Br^-]{e^-,N_2} Mo^0(N_2)_3$$

2   **3**   **3-N₂**   **9**   **6**

$^1/_2 N_2 \rightleftarrows -^1/_2 N_2$

Mo = $(^{py}PNP)Mo$

$^1/_2 [Mo^{II}Br_2]_2(N_2)$
5^{t,t}

2 or 5^{t,t}

$^1/_2 N_2 \mid -^1/_2 N_2$ $^1/_2 N_2 \mid -^1/_2 N_2$

2 or 5^{t,t}

$2e^-$
$^1/_2 N_2$
$- 2Br^-$

$Mo^{IV}Br(N)$ **4** ← $^1/_2 [Mo^IBr]_2(N_2)$ $^1/_2 [Mo^0(N_2)_2]_2(N_2)$

7   **1**

overall electrochemical
*N₂ spitting reaction*

in the bulk solution

in **Scheme 5**, one pathway takes place entirely in the vicinity of the electrode surface, while the other pathway features comproportionation chemical redox reactions that generate **4** away from the electrode surface. This spatial separation of different reaction pathways is a consequence of the inherent heterogeneity of electron transfer reactions at solid electrode surfaces.

The initial reductive N_2 activation steps, which occur near the electrode surface, are identical for the two pathways. Cyclic voltammetry studies establish that reduction of **2** triggers Br^- dissociation to generate the 5-coordinate species $(^{py}PNP)MoBr_2$ (**3, Scheme 5**, $\Delta G_{Br,diss}° = -2$ kcal/mol). N_2 association to **3** generates **3-N₂** (for *cis*-**3-N₂**, $\Delta G_{N2binding}° = 6$ kcal/mol; for *trans*-**3-N₂**, $\Delta G_{N2binding}° = 7$ kcal/mol), which is in equilibrium with the bimetallic species *trans,trans*-$[(^{py}PNP)MoBr_2]_2(\mu-N_2)$ and free N_2 (**5^{t,t}, Scheme 5**). The monometallic-bimetallic equilibrium heavily favors **5^{t,t}** ($\Delta G_{dimerization}° = -4$ or -5 kcal/mol depending on isomer of **3-N₂**), consistent with the detection of **5^{t,t}** at the electrode surface during SEC experiments.

Although **5^{t,t}** is the dominant Mo^{II} species, this complex has a highly negative reduction potential, and electrolysis at such negative potentials results in significantly decreased yields of **4** (**Table 1**, above). The monometallic-bimetallic equilibrium is therefore essential because it enables subsequent reduction to proceed via a CE mechanism: **5^{t,t}** dissociates and binds N_2 to generate **3-N₂**, which undergoes $1e^-$ reduction at milder potentials and after loss of a bromide anion, generates the 5-coordinate Mo^I species $(^{py}PNP)MoBr(N_2)$ (**8, Scheme 6**). Coordination of a second N_2 ligand to form *trans*-$(^{py}PNP)MoBr(N_2)_2$ (**9, Scheme 6**) was computed to be exergonic and kinetically facile ($\Delta G_{N2binding}° = -8$ kcal/mol and $\Delta G_{N2binding}^{\ddagger} = 10$ kcal/mol). This sequence aligns with the recently reported isolation of *trans*-$(^{py}PNP)MoI(N_2)_2$.[25]

Scheme 6. Stepwise formation of $(^{py}PNP)Mo(N)Br$ (**4**) at the electrode surface upon reduction of $(^{py}PNP)MoBr_2(N_2)$ (**3-N₂**).
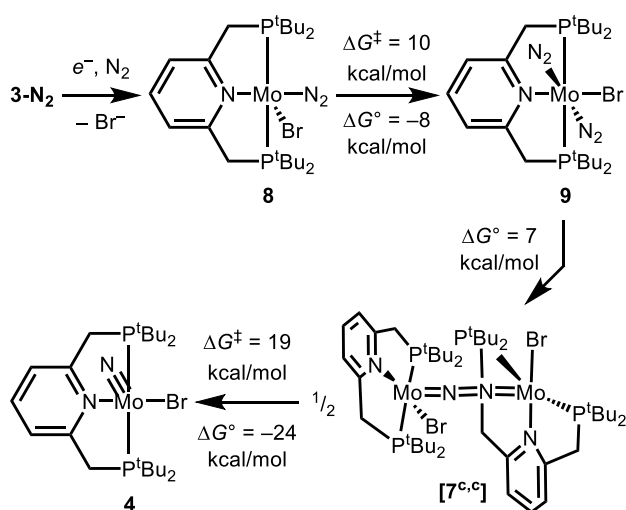
After formation of **9**, the two reaction pathways bifurcate. Focusing first on the bulk solution pathway, the Mo^I species **9** is further reduced at the electrode surface to yield the bimetallic Mo^0 species, **1**. Complex **1** and its monometallic equilibrium partner $(^{py}PNP)Mo(N_2)_3$ (**6**) are indeed the dominant Mo species detected by UV-vis, IR, and rR SEC experiments (**Scheme 5**). These Mo^0 species do not thermally split N_2 into nitride complexes. However, as they diffuse away from the electrode into the bulk solution, they can participate in chemical redox reactions with **2** or **5^{t,t}** via comproportionation to generate the bimetallic $Mo^{I/I}$ complex **7^{c,c}** (**Scheme 5**, $\Delta G_{2,comp}° = 11$ kcal/mol per equivalent of **7^{c,c}** formed). Subsequent N–N bond cleavage from **7^{c,c}** to yield **4** was computed to be kinetically accessible ($\Delta G_{cleave}^{\ddagger} = 19$ kcal/mol) and thermodynamically favorable (($\Delta G_{cleave}° = -24$ kcal/mol). Yoshizawa and Nishibayashi have proposed that the iodide analogue of **7^{c,c}** is the species responsible for N_2 cleavage in the reduction of

N2 to give ammonia catalyzed by (pyPNP)MoI3.[25] Experimental support for the bulk solution pathway arises from time courses showing that **1** reacts after the applied potential is released in SEC experiments, and from chemical comproportionation reactions of **1** and either **2** or **5^{t,t}**, which form **4** in the absence of an applied potential. These chemical redox pathways can "rescue" over-reduced Mo complexes to generate the Mo^I intermediates active for N2 splitting.

In the pathway proceeding in the reaction–diffusion layer near the electrode surface, the Mo^I species **9** loses N2 and undergoes bimolecular formation of the N2-bridged complex **7^{c,c}** (**Scheme 6**, $\Delta G_{formation}° = 7$ kcal/mol), which cleaves N2 as described above to form nitride **4** near the electrode surface. The more stable *trans* isomer of **9** should lead directly to the *cis,cis* isomer **7^{c,c}** that is proposed to be the active geometric isomer for thermal N2 splitting (**Scheme 6**). This pathway must be viable because reduction of **5^{t,t}** under an Ar atmosphere yields **4**. Under Ar, there is no N2 available to support over-reduction to **1**, thus precluding any chemical redox reactions. Instead, **5^{t,t}** must be reduced to **7^{c,c}** in the reaction layer, followed by N2 splitting. In fact, a feature consistent with **4** appears in the return sweep of CVs of **5^{t,t}**, consistent with N2 splitting in the reaction layer (**Figure S57**).

The two pathways for electrochemical N2 splitting are likely both operating during electrolysis. The dominant path will depend on the relative rate of (a) the chemical formation of **7^{c,c}** from **9**, and (b) the electrochemical reduction of **9** to Mo^0 complexes **6** and **1**. A change in dominant nitride synthesis path may be reflected in the data of **Table 1** (above). For example, the yields of **4** drop considerably when more negative applied potentials are employed, suggesting that over-reduction dominates and comproportionation pathways are predominantly responsible for generating **4**. Conversely, the yield of **4** is higher when N2-bridged complex **5^{t,t}** undergoes CPE under Ar (with N2 splitting at the electrode surface) than under N2 (where over-reduction necessitates chemical redox pathways).

3. CONCLUSIONS

The viability of electrochemical N2 binding and splitting by the molybdenum(III) pincer complex, (pyPNP)MoBr3 is established in this work. The N2-derived nitride (pyPNP)Mo(N)Br was actually produced in higher yields during electrolysis (41%) than when chemical reductants are used (20%). Employing a suite of electrochemical, spectroscopic, and computational methods provides a detailed account of the electroreductive N2 splitting mechanism: initial reduction of (pyPNP)MoBr3 generates Mo^I species at the electrode surface that can either (a) form N2-bridged intermediates that cleave N2 in the reaction–diffusion layer near the electrode surface, or (b) be further electroreduced to Mo^0 species that undergo *chemical* redox reactions with higher-valent Mo species to generate the desired nitride product in the bulk solution. These comproportionation reactions can be directly observed in the bulk solution, far from the electrode surface, in the absence of an applied potential.

The electrochemical yield of (pyPNP)Mo(N)Br was found to be strongly dependent on applied potential, with higher yields of nitride obtained at less negative potentials. Two key mechanistic features contribute to this observation: first is the potential inversion that occurs upon binding of N2, which helps lower the necessary applied potential for the second and third electron transfer events. Secondly, the presence of rapid monometallic-bimetallic complex equilibria plays a role. At more negative potentials, bimetallic Mo^{II} species can be reduced directly, and the resulting Mo^I species are rapidly converted to Mo^0 (perhaps because they are in a *trans,trans* geometry coming from **5^{t,t}**, slowing the rate of N2 splitting) — thereby precluding N2 splitting at the electrode surface.

Another distinct feature of the discovered electrochemical mechanism of N2 cleavage is the spatial evolution of the reaction. Near the electrode surface, Mo^I species face a kinetic competition between (a) formation of the N2-bridged intermediate capable of splitting into nitride complexes, and (b) over-reduction to Mo^0 species. Once Mo^0 species are generated, no further reaction at the electrode surface is possible. As the Mo^0 species diffuse away from the electrode and into the bulk solution, however, chemical redox reactions with starting material can take place to re-form Mo^I species and eventually split N2. It is not without irony that an "electrochemical" N2 splitting reaction relies on a chemical redox reaction! This also provides a key lesson for future electrochemical mechanistic investigations: researchers cannot solely focus on reactions occurring within the reaction layer near the electrode surface. Spectroscopic probes both near the electrode surface and in the bulk solution can provide complementary mechanistic insights during electrolyses.

The intermediacy of Mo^0 complex **1** in an N2 splitting pathway also raises important questions about mechanisms of ammonia synthesis. We have shown that either chemical oxidants (Mo^{III} or Mo^{II} species) or a lutidinium acid commonly used in catalytic N2 fixation can react with **1** to generate (pyPNP)Mo(N)Br. Complex **1** is representative of a wide class of low-valent Mo complexes that have been proposed to reduce N2 via the so-called "distal pathway" first proposed by Chatt. Mechanistic studies demonstrate that **1** can participate in an N2 splitting pathway.

Demonstrating electrochemical N2 splitting at molybdenum ultimately led us to elucidate unanticipated mechanistic aspects that can guide catalyst development.

ASSOCIATED CONTENT

Supporting Information
Experimental details and characterization data (PDF)

Coordinates of optimized geometries in compressed .mol format (ZIP)

AUTHOR INFORMATION

Corresponding Author

* A.J.M.M. Email: ajmm@email.unc.edu

REFERENCES

(1)   Vaclav, S. Detonator of the Population Explosion. *Nature* **1999**, *400*, 415.

(2)   Erisman, J. W.; Sutton, M. A.; Galloway, J.; Klimont, Z.; Winiwarter, W. How a Century of Ammonia Synthesis Changed the World. *Nat. Geosci.* **2008**, *1*, 636–639.

(3)   Renner, J. N.; Greenlee, L. F.; Herring, A. M.; Ayers, K. E. Electrochemical Synthesis of Ammonia: A Low Pressure, Low Temperature Approach. *Electrochem. Soc. Interface* **2015**, *24*, 51–57.

(4)   Tallaksen, J.; Bauer, F.; Hulteberg, C.; Reese, M.; Ahlgren, S. Nitrogen Fertilizers Manufactured Using Wind Power: Greenhouse Gas and Energy Balance of Community-Scale Ammonia Production. *J. Clean. Prod.* **2015**, *107*, 626–635.

(5)   Hochman, G.; Goldman, A.; Felder, F. A.; Mayer, J.; Miller, A.; Holland, P. L.; Goldman, L.; Manocha, P.; Song, Z.; Aleti, S. The Potential Economic Feasibility of Direct Electrochemical Nitrogen Reduction as a Route to Ammonia. *ACS Sustain. Chem. Eng.* **2020**, *8*, 8938–8948.

(6)   Dmitry V. Yandulov; Schrock, R. R. Catalytic Reduction of Dinitrogen to Ammonia at a Single Molybdenum Center. *Science* **2003**, *301*, 76–78.

(7)   Eizawa, A.; Nishibayashi, Y. Catalytic Nitrogen Fixation Using Molybdenum–Dinitrogen Complexes as Catalysts. In *Topics in Organometallic Chemistry*; Springer Verlag, 2017; Vol. 60, pp 153–169.

(8)   Ashida, Y.; Nishibayashi, Y. Catalytic Conversion of Nitrogen Molecule into Ammonia Using Molybdenum Complexes under Ambient Reaction Conditions. *Chem. Commun.* **2021**, *57*, 1176–1189.

(9)   Bennaamane, S.; Espada, M. F.; Mulas, A.; Personeni, T.; Saffon-Merceron, N.; Fustier-Boutignon, M.; Bucher, C.; Mézailles, N. Catalytic Reduction of N_2 to Borylamine at a Molybdenum Complex. *Angew. Chem. Int. Ed.* **2021**, *60*, 20210–20214.

(10)   Pickett, C. J.; Talarmin, J. Electrosynthesis of Ammonia. *Nature* **1985**, *317*, 652–653.

(11)   Chalkley, M. J.; Del Castillo, T. J.; Matson, B. D.; Peters, J. C. Fe-Mediated Nitrogen Fixation with a Metallocene Mediator: Exploring PK_a Effects and Demonstrating Electrocatalysis. *J. Am. Chem. Soc.* **2018**, *140*, 6122–6129.

(12)   Lindley, B. M.; van Alten, R. S.; Finger, M.; Schendzielorz, F.; Würtele, C.; Miller, A. J. M.; Siewert, I.; Schneider, S. Mechanism of Chemical and Electrochemical N_2 Splitting by a Rhenium Pincer Complex. *J. Am. Chem. Soc.* **2018**, *140*, 7922–7935.

(13)   Sherbow, T. J.; Thompson, E. J.; Arnold, A.; Sayler, R. I.; Britt, R. D.; Berben, L. A. Electrochemical Reduction of N_2 to NH_3 at Low Potential by a Molecular Aluminum Complex. *Chem. – A Eur. J.* **2019**, *25*, 454–458.

(14)   Katayama, A.; Ohta, T.; Wasada-Tsutsui, Y.; Inomata, T.; Ozawa, T.; Ogura, T.; Masuda, H. Dinitrogen-Molybdenum Complex Induces Dinitrogen Cleavage by One-Electron Oxidation. *Angew. Chem. Int. Ed.* **2019**, *58*, 11279–11284.

(15)   van Alten, R. S.; Wätjen, F.; Demeshko, S.; Miller, A. J. M.; Würtele, C.; Siewert, I.; Schneider, S. (Electro-)Chemical Splitting of Dinitrogen with a Rhenium Pincer Complex. *Eur. J. Inorg. Chem.* **2020**.

(16)   Arashiba, K.; Miyake, Y.; Nishibayashi, Y. A Molybdenum Complex Bearing PNP-Type Pincer Ligands Leads to the Catalytic Reduction of Dinitrogen into Ammonia. *Nat. Chem.* **2011**, *3*, 120–125.

(17)   Chatt, J. A Possible Mimic of the Nitrogenase

Reaction; 1980; pp 379–391.

(18) Schrock, R. R. Catalytic Reduction of Dinitrogen to Ammonia at a Single Molybdenum Center. *Acc. Chem. Res.* **2005**, *38*, 955–962.

(19) Tanaka, H.; Arashiba, K.; Kuriyama, S.; Sasada, A.; Nakajima, K.; Yoshizawa, K.; Nishibayashi, Y. Unique Behaviour of Dinitrogen-Bridged Dimolybdenum Complexes Bearing Pincer Ligand towards Catalytic Formation of Ammonia. *Nat. Commun. 2014 51* **2014**, *5*, 1–11.

(20) Kuriyama, S.; Arashiba, K.; Nakajima, K.; Tanaka, H.; Kamaru, N.; Yoshizawa, K.; Nishibayashi, Y. Catalytic Formation of Ammonia from Molecular Dinitrogen by Use of Dinitrogen-Bridged Dimolybdenum-Dinitrogen Complexes Bearing PNP-Pincer Ligands: Remarkable Effect of Substituent at Pnp-Pincer Ligand. *J. Am. Chem. Soc.* **2014**, *136*, 9719–9731.

(21) Arashiba, K.; Eizawa, A.; Tanaka, H.; Nakajima, K.; Yoshizawa, K.; Nishibayashi, Y. Catalytic Nitrogen Fixation via Direct Cleavage of Nitrogen–Nitrogen Triple Bond of Molecular Dinitrogen under Ambient Reaction Conditions. *Bull. Chem. Soc. Jpn.* **2017**, *90*, 1111–1118.

(22) Ashida, Y.; Arashiba, K.; Nakajima, K.; Nishibayashi, Y. Molybdenum-Catalysed Ammonia Production with Samarium Diiodide and Alcohols or Water. *Nature* **2019**, *568*, 536–540.

(23) Elgrishi, N.; Kurtz, D. A.; Dempsey, J. L. Reaction Parameters Influencing Cobalt Hydride Formation Kinetics: Implications for Benchmarking H_2-Evolution Catalysts. *J. Am. Chem. Soc.* **2017**, *139*, 239–244.

(24) Savéant, J.; Costentin, C. Elements of Molecular and Biomolecular Electrochemistry; Wiley, 2019.

(25) Arashiba, K.; Tanaka, H.; Yoshizawa, K.; Nishibayashi, Y. Cycling between Molybdenum-Dinitrogen and -Nitride Complexes to Support the Reaction Pathway for Catalytic Formation of Ammonia from Dinitrogen. *Chem. – A Eur. J.* **2020**, *26*, 13383–13389.

(26) Al-Salih, T. I.; Pickett, C. J. Electron-Transfer Reactions in Nitrogen Fixation. Part 1. The Electrosynthesis of Dinitrogen, Hydride, Isocyanide, and Carbonyl Complexes of Molybdenum: Intermediates, Mechanisms, and Energetics. *J. Chem. Soc. Dalt. Trans.* **1985**, *53*, 1255.

(27) Kirchhoff, J. R.; Heineman, W. R.; Deutsch, E. Technetium Electrochemistry. 4. Electrochemical And Spectroelectrochemical Studies On The Bis(Tertiary Phosphine Or Arsine (D))Rhenium(III) Complexes Trans - [Red₂X₂]+ (X = Cl, Br). Comparison With The Technetium(III) Analogues. *Inorg. Chem.* **1987**, *26*, 3108–3113.

(28) Lever, A. B. P. Electrochemical Parametrization

of Rhenium Redox Couples. *Inorg. Chem.* **1991**, *30*, 1980–1985.

(29) Peters, J. C.; Cherry, J.-P. F.; Thomas, J. C.; Baraldo, L.; Mindiola, D. J.; Davis, W. M.; Cummins, C. C. Redox-Catalyzed Binding of Dinitrogen by Molybdenum N-Tert-Hydrocarbylanilide Complexes: Implications for Dinitrogen Functionalization and Reductive Cleavage. **1999**.

(30) Rittle, J.; McCrory, C. C. L.; Peters, J. C. A 10^6-Fold Enhancement in N_2-Binding Affinity of an $Fe_2(\mu$-$H)_2$ Core upon Reduction to a Mixed-Valence $Fe^{II}Fe^{I}$ State. *J. Am. Chem. Soc.* **2014**, *136*, 13853–13862.

(31) Clouston, L. J.; Bernales, V.; Carlson, R. K.; Gagliardi, L.; Lu, C. C. Bimetallic Cobalt-Dinitrogen Complexes: Impact of the Supporting Metal on N_2 Activation. *Inorg. Chem.* **2015**, *54*, 9263–9270.

(32) Del Castillo, T. J.; Thompson, N. B.; Peters, J. C. A Synthetic Single-Site Fe Nitrogenase: High Turnover, Freeze-Quench ^{57}Fe Mössbauer Data, and a Hydride Resting State. *J. Am. Chem. Soc.* **2016**, *138*, 5341–5350.

(33) Bezdek, M. J.; Guo, S.; Chirik, P. J. Terpyridine Molybdenum Dinitrogen Chemistry: Synthesis of Dinitrogen Complexes That Vary by Five Oxidation States. *Inorg. Chem.* **2016**, *55*, 3117–3127.

(34) Rafiq, S.; Bezdek, M. J.; Chirik, P. J.; Scholes, G. D. Dinitrogen Coupling to a Terpyridine-Molybdenum Chromophore Is Switched on by Fermi Resonance. *Chem* **2019**, *5*, 402–416.

(35) Arashiba, K.; Kuriyama, S.; Nakajima, K.; Nishibayashi, Y. Preparation and Reactivity of a Dinitrogen-Bridged Dimolybdenum-Tetrachloride Complex. *Chem. Commun.* **2013**, *49*, 11215–11217.

(36) Holland, P. L. Metal-Dioxygen and Metal-Dinitrogen Complexes: Where Are the Electrons? *Dalton Trans.* **2010**, *39*, 5415–5425.

(37) Krejčik, M.; Daněk, M.; Hartl, F. Simple Construction of an Infrared Optically Transparent Thin-Layer Electrochemical Cell. Applications to the Redox Reactions of Ferrocene, Mn₂(CO)₁₀ and Mn(CO)₃ (3,5-Di-t-Butyl-Catecholate)⁻. *J. Electroanal. Chem. Interfacial Electrochem.* **1991**, *317*, 179–187.

(38) Bruch, Q. J.; Connor, G. P.; Chen, C.-H.; Holland, P. L.; Mayer, J. M.; Hasanayn, F.; Miller, A. J. M. Dinitrogen Reduction to Ammonium at Rhenium Utilizing Light and Proton-Coupled Electron Transfer. *J. Am. Chem. Soc.* **2019**, *141*, 20198–20208.

(39) Yamout, L. S.; Ataya, M.; Hasanayn, F.; Holland, P. L.; Miller, A. J. M.; Goldman, A. S. Understanding Terminal versus Bridging End-on N_2 Coordination in Transition Metal Complexes. *J. Am. Chem. Soc.* **2021**, *143*, 9744–9757.

(40)   Liao, Q.; Saffon-Merceron, N.; Mézailles, N. N_2 Reduction into Silylamine at Tridentate Phosphine/Mo Center: Catalysis and Mechanistic Study. *ACS Catal.* **2015**, *5*, 6902–6906.

(41)   Kuriyama, S.; Arashiba, K.; Nakajima, K.; Tanaka, H.; Yoshizawa, K.; Nishibayashi, Y. Azaferrocene-Based PNP-Type Pincer Ligand: Synthesis of Molybdenum, Chromium, and Iron Complexes and Reactivity toward Nitrogen Fixation. *Eur. J. Inorg. Chem.* **2016**, *2016*, 4856–4861.

(42)   Mastragostino, M.; Nadjo, L.; Saveant, J. M. Disproportionation and ECE Mechanisms—I. Theoretical Analysis. Relationships for Linear Sweep Voltammetry. *Electrochim. Acta* **1968**, *13*, 721–749.

Electrochemical N₂ Cleavage

"Over-reduction" to Mo⁰ at the electrode surface

Comproportionation-induced N₂ splitting in the bulk solution

key intermediate detected via spectroelectrochemical UV-Vis, IR, and rR